On dimensional reduction in multiscale, finite element and atomistic, analysis in solid mechanics

DUBRAVKA MIJUCA
Department of Mechanics, Faculty of Mathematics
University of Belgrade
Studentski trg 16, 11000 Belgrade
SERBIA

Abstract: - In the present paper it will be shown how dimensional reduction theories can drastically deteriorate the place and intensity of maximal stress results, which can lead to the premature structure failure. In addition, bridging of continuum (finite element) and atomistic (molecular dynamics) mechanics is more accurate if continuum approach is based on reliable fully three-dimensional numerical approach, mainly because it prevail spurious results and enable extension of the continuum region deep toward the atomistic scale. It is primarily because in reliable finite element approaches we can benefit from robust finite element behavior in which aspect ratio of finite element can be drastically increased and near incompressibility can be traced without suffering from locking effects. Keeping in mind that dimensional reduction approaches are traditionally established only because of the faster and easier hand-out and early computer calculations of the mechanical systems, the goal of the present paper is to prove that it is possible to develop numerical procedure which is both, based on the full multifield mixed theories and time efficient, and also reliable throughout the scales. Presently, the reliable primal-mixed finite element approach in semi coupled thermo-mechanical analysis is used for comparison.

Key-Words: – solid mechanics, dimensional reduction, finite element, multiscale, geometric invariance, incompressible limit, residual stresses

1 Introduction

When it comes to numerical simulation [1], i.e. approximation of the mathematical model given by differential equations by some chosen numerical method, the accuracy of the numerical results strongly depends on the reliability [2] of the numerical scheme, quality of the material's characterization and model idealization (dimensional reduction and detail suppression technique). The finite element (FE) method is certainly the first numerical method of choice in thermo-mechanical analysis of solid bodies for several decades. Although, theoretical settings of different approaches, as primal, mixed [3] and hybrid, were simultaneously developed, only primal approach, were there is only one solution variable, gained greater attention of the industry and commercial software developers. In addition, the finite elements based on dimensional reduction [4] theories (beam and plane) are still the most used elements. It is primarily due to the limitation of the speed of the available computer recourses and opinion that is not possible to develop reliable mixed approaches in which displacement and stresses are simultaneous calculated. Nevertheless, new materials, as composite sandwiched plates with foam in its core, functionally graded materials, and analysis at higher temperatures (fire) when material properties drastically change, require the fully 3d reliable numerical procedure toward incompressibility [5, 6]. Next, the use of mixed/hybrid FE approaches [7. 8] is favorable because of the possibility to introduce *a priori* known stresses, as residual, directly in calculation as the known initial conditions. It is opposite to primal approaches (e.g. displacement finite element method) in which initial stresses are introduced as a contribution to the force vector, while residual stresses are simply added *a posteriori* to calculated stresses, which entails a lost the accuracy and is applicable only in elastic range. Further, when the state of the initial stress is heterogeneous along the thickness it is not possible to use plate theories, even if the theory behind is mixed. Further reason against the use of plane theories is so-called locking effects which slowed convergence [8]. A similar effect called volumetric or dilatational locking is widely known in relation to

weakly compressible bodies. Under certain conditions, even the classical model based on the Kirchoff–Love hypotheses may lead to membrane locking. Though there are new approaches proposed to improve the convergence of numerical solution for new classes of problems for thin and nonthin shells with a curvilinear (circular, elliptical) hole, and different types modern methods overcome the locking [8], all of them rely on some artificial stabilization techniques which deteriorate reliability.
Let's emphasize that design benchmark examples which go in hand to plane theories, are mainly responsible for the wide popularity of the dimensional reduction theories in engineering numerical calculation.
Nowadays the speed and cost of the modern PC computers are of the best supercomputers in the past. Next, the highly time efficient numerical procedures for the solution of the large scale systems are available [9]. Further, the number of mixed and hybrid and multifield coupled approaches are proposed [ja, barbara]. Even more, there is a growing need for the multiscale [10] and micro-macro approaches [6], because it is still difficult to inflate atomistic models to the size of specimens and components..
In the present paper it will be shown that by the use of the multifield primal-mixed finite approach [11, 12, 13] which has all variable of interest, temperature, heat flux, displacement and stress as solution variable, all above shortcomings are cured and the approach is reliable, time efficient and adequate for atomistic coupling. It is shown that present multiscale numerical approach, based on one-to-one correspondence between molecular dynamics on atomistic scale and primal-mixed finite element scheme on macroscale, is reliable and efficient. The seamless semi-coupling between length scales is achieved. Presently, the original primal-mixed finite element method is used, to describe the nonlinear deformation behavior of materials at the local macroscopic scales, that is, on continuum-mechanics-based framework, while molecular dynamics and embedded-atom interatomic potential is used on atomic scale. The reliability of present approach relies on robustness of primal-mixed finite element scheme, which is insensitive to distortion of the finite element in the mesh and high ratio of its maximal and minimal axial dimensions. The reliability of the present primal-mixed FE approach is proven in [11] and [13].

2 Dimensional reduction

Dimensional reduction is one of two generic techniques for model idealization [14]. The solid bodies with one or two axial dimensions much smaller than other are traditionally examined by plate, shell or beam theories based on dimensional and solution variable reduction in the direction normal to middle surface, or beam's cross section, respectively. Obviously, these geometrical simplifications produce errors in final solution, which are traditionally considered to be negligible. From the historical point of view, plate, shell and beam theories were needed to enable simplified engineering calculations. On the other hand, in order to capture stress concentrations at local details, it is often desirable to combine the reduced dimensional element types with higher dimensional elements, like hexahedral, in the whole global model. Consequently, it requires some scheme for coupling the element types that conforms to the governing equations of the problem, which do not introduce any spurious results of dual variable (stress, heat flux) at the dimensional interface. However, regardless of coupling technique there will be some so-called *transition error* introduced.
Theories based on dimensional reduction suffer from the aspect-ratio restriction, which is highly inappropriate in multiscale analysis, where atomistic region is bridged to continuum region and therefore very narrow finite elements are welcomed. In addition, these theories are inappropriate in analysis of coated bodies or thin films of micron sized and less.
Nevertheless, idealization of geometry in order to reduce the complexity of the model is the major factor limiting the wider application of FEA in computational materials technology where material is respected throughout the dimensional scales. In addition, in the case when finite element approach is primal, model problem is approximated by plates or shells, and material undergoes plastic deformation or applied external loading produce excessive bending, the system matrix will become highly ill-conditioned.

3 Multiscale robustness

There is a growing need to develop systematic modelling and simulation approaches for multiscale multimaterials model problems to provide the accurate data about the state of stress, defect structure, thermal and mechanical performance of the subregions with different geometric scales. These problems arose, for example, in the analysis of coated components, where materials scientist use

soft, hard, biomimetic, wear resistant or corrosion protecting multiphase or multilayer coatings to gain significant performance advantages (e.g. thermal coating of metal based turbines with some ceramics). The other example is multi-layered microelectronic packaging or wind turbines, where interfacial stress induced by thermal loading or moisture during manufacturing or exploitation is responsible for delamination-related failures.

Reliability of the present FE HC8/27 makes it a candidate of the first choice for the use in thermo-mechanical multiscale analysis, such as aforementioned examples where high aspect ratio of FE is inevitable. The reliable use of present approach in multiscale analysis where outer layers of materials are of microscale is demonstrated in [13].

4 Primal-mixed formulation

The transient thermoelastic problem [11, 13] consists in determining the response of the body in terms of displacement $\boldsymbol{u}$, temperature T, stress $\boldsymbol{t}$ and heat flux $\boldsymbol{q}$, according to the compatibility equations, equilibrium and thermal balance equations, constitutive equations and boundary and initial conditions. The detailed description of the present field equations one may find in [11], where it is shown that original and reliable transient heat transfer and mechanical primal-mixed finite element approaches result with next linear equation systems, respectively:

$$\begin{bmatrix} \mathrm{A}_{vv} & -\mathrm{D}_{vv} \\ -\mathrm{D}_{vv}^{\ T} & 0 \end{bmatrix} \begin{bmatrix} \mathbf{t}_v \\ \mathbf{u}_v \end{bmatrix} = \begin{bmatrix} -\mathrm{A}_{vp} & \mathrm{D}_{vp} \\ \mathrm{D}_{pv}^{\ T} & 0 \end{bmatrix} \begin{bmatrix} \mathbf{t}_p \\ \mathbf{u}_p \end{bmatrix} - \begin{bmatrix} \mathbf{0} \\ \mathbf{f}_p + \mathbf{p}_p \end{bmatrix}. \quad (1)$$

$$\begin{bmatrix} \mathrm{M}_{vv} & \mathrm{B}_{vv}^{\ T} \\ \mathrm{B}_{vv} & -\mathrm{D}_{vv} - \mathrm{S}_{vv} \end{bmatrix} \begin{bmatrix} \mathbf{q}_v \\ \mathrm{T}_v \end{bmatrix} = \begin{bmatrix} -\mathrm{M}_{vp} & -\mathrm{B}_{vp}^{\ T} \\ -\mathrm{B}_{vp} & \mathrm{D}_{vp} \end{bmatrix} \begin{bmatrix} \mathbf{q}_p \\ \mathrm{T}_p \end{bmatrix} + \begin{bmatrix} 0 & 0 \\ 0 & \mathrm{S}_{vp} \end{bmatrix} \begin{bmatrix} 0 \\ \mathrm{T}_p^{(t-1)} \end{bmatrix} + \begin{bmatrix} 0 \\ \mathrm{F}_p + \mathrm{H}_p - \mathrm{K}_p \end{bmatrix} + \begin{bmatrix} 0 \\ -\mathrm{L}_p^{(t-1)} \end{bmatrix}, \quad (2)$$

Where,

$$A_{\Lambda u v \Gamma s t} = \sum_e \int_{\Omega_i} \Omega_\Lambda^N S_N g^a_{(\Lambda)u} g^b_{(\Lambda)v} A_{abcd} g^c_{(\Gamma)s} g^d_{(\Gamma)t} T_L \Omega_\Gamma^L d\Omega$$

$$D^{\Gamma q}_{\Lambda u v} = \sum_e \int_{\Omega_\square} \Omega_\Lambda^N S_N U_a^K \Omega_K^\Gamma g^a_{(\Lambda)u}\ g^{(\Gamma)q}_{(\Lambda)v} d\Omega$$

$$f^{\Lambda q} = \sum_e \int_{\Omega_\square} g_a^{(\Lambda)q} \Omega_M^\Lambda V^M f^a d\Omega$$

$$p^{\Lambda q} = \sum_e \int_{\partial\Omega_u} g_a^{(\Lambda)q} \Omega_M^\Lambda V^M p^a d\partial\Omega \quad (3)$$

and

$$M_{\Lambda p \Gamma r} = \sum_e \int_{\Omega_e} \overset{(e)}{\Omega}{}_\Lambda^L\ g^a_{(L)p} V_L k^{-1}_{ab} g^b_{(M)r} V_M\ \overset{(e)}{\Omega}{}_\Gamma^M\ d\Omega_e;$$

$$B_{\Lambda p \Gamma} = \sum_e \int_{\Omega_e} \overset{(e)}{\Omega}{}_\Lambda^L\ g^a_{(L)p} V_L P_{M,a}\ \overset{(e)}{\Omega}{}_\Gamma^M\ d\Omega_e$$

$$D_{\Lambda\Gamma} = \sum_e \int_{\partial\Omega_{ce}} h_c\ \overset{(e)}{\Omega}{}_\Lambda^L\ P_L P_M\ \overset{(e)}{\Omega}{}_\Gamma^M\ \partial\Omega_{ce};$$

$$S_{\Lambda\Gamma} = \sum_e \int_{\Omega_e} \frac{\rho c}{\Delta t} \overset{(e)}{\Omega}{}_\Lambda^L\ P_L P_M\ \overset{(e)}{\Omega}{}_\Gamma^M\ d\Omega_e; \quad (4)$$

$$L_\Gamma = \sum_e \int_{\Omega_e} \frac{\rho c}{\Delta t}\ {}^{n-1}T_{(M)}\ P_M\ \overset{(e)}{\Omega}{}_\Gamma^M\ d\Omega_e$$

$$F_\Gamma = \sum_e \int_{\Omega_e} \overset{(e)}{\Omega}{}_\Gamma^M\ P_M f d\Omega_e,\ H_\Gamma = \sum_e \int_{\partial\Omega_{he}} \overset{(e)}{\Omega}{}_\Gamma^M\ P_M h\, d\partial\Omega_{he};$$

$$K_\Gamma = \sum_e \int_{\partial\Omega_{ce}} \overset{(e)}{\Omega}{}_\Gamma^M\ P_M h_c T_a\, d\partial\Omega_{ce}$$

It is obvious from (1) and (2) that present primal-mixed finite element approaches represent a saddle point problems, where system matrix is indefinite with additional sparsity concerning zeroes diagonal entries. Solvers MA57 and MA47 from *Harwell Subroutine Library*, which are designed for the solution of this kind of systems, are chosen as suitable for testing. They are based on the multifrontal method that is direct approach for solving linear systems of equations. Like most sparse direct solvers, algorithms are developed in three distinct computational phases: analyze, factorize and solve phase [15].

5 Numerical examples

The next three benchmark model problems are specially chosen to show that plane theory and resulting plane FE analysis, can mislead design engineers in the behavior of the considered structure. We will show that full approximation of stresses using the hexahedral finite elements based on the primal-mixed formulations give us realistic behavior of the structure.

5.1 Clamped square plate

By the next two examples we will show by the use of the full mechanical theory that, the usual premise that stress concentration point of a clamped plate is on the clamped edge is not correct.

5.1.1 Clamped square plate

A clamped square plate model problem [11, 16] with edge length $a = 2$ and thickness $t = 0.01$, subjected to the uniform pressure $q = -100$, is considered. The Young's modulus is $E = 1.7472 \cdot 10^7$, and Poisson's ratio is $\nu = 0.3$. The analytical solution for the

maximal deflection at the plate centre C calculated by the Kirchhoff's plate theory is w=1.26 [26]. Axial dimension of the finite elements in the transversal direction is $(1/100)/2 = 0.005$. Only a quarter of the plate, shown in Figure 12, was analysed due to the symmetry. The essential stress boundary conditions $t^{zz}\big|_{z=0.01} = -100$ are prescribed at the nodes lying on the upper surface of the plate. The present model problem was discretized by the sequence of meshes with two layers of brick finite elements HC8/9 per thickness, that is $N \times N \times 2$.

Further, clamped edges were simulated by zeroing degrees of freedom connected to the displacement ($u_x = u_y = u_z = 0$) and transversal shear stress components $t^{xy} = 0$, only. This case, denoted as the Case A, is shown in Figure 1.

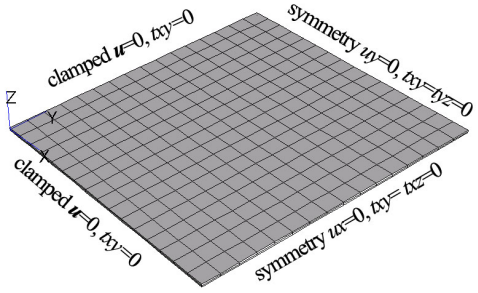

Fig. 1. Clamped plate finite element model – case A

The visualization of the stress pattern for the FE mesh $N = 32$ for the case A, that is, full theory, is shown in Figure 2. We can see that stress concentration point is not at the clamped edge, but in its vicinity:

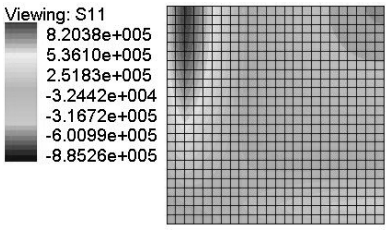

Fig. 2. Case A: the stress concentration point

If we want to simulate the *plate theory*, under which stress concentration point is on the clamped edge, all transversal shear stress components (t^{xy}, t^{xz} and t^{yz}) must be suppressed (set to zero) at least at the clamped edge (or in the whole plate), That case is denoted as Case B.

The visualization of the stress pattern for the FE mesh $N = 32$, where plane theory assumption that shear stress components are neglected, is shown in Figure 4. We can see that stress concentration point is at clamped edge.

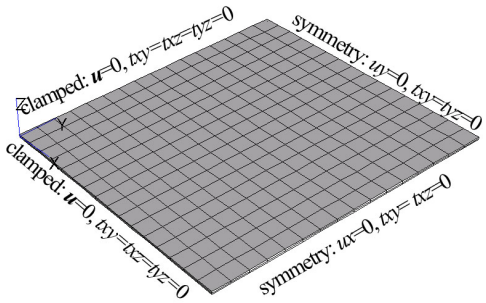

Fig. 3. Clamped plate finite element model – case B

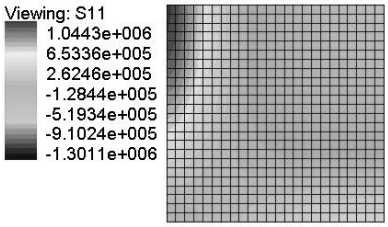

Fig. 4. Case B: the stress concentration point

The detailed study of the convergence for the present model problem can be found in [11]. Nevertheless, let's discuss convergence shown in Fig. 5.

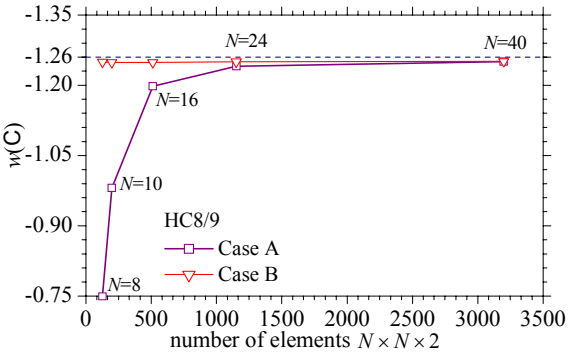

Fig. 5. Clamped square plate: maximal deflection

From the numerical result obtained by the present method in the case A, we may see that target results converge from below to the solution that is a little bit lower than one obtained by the Kirchhoff's plate theory. On the other hand, in the case B, where the assumptions of the plate theory were respected as much as possible, the target results for the sequence of refined meshes instantly converge to the solution which is a little bit less than one obtained by the Kirchhoff's plate theory. The possible explanation for that phenomenon is that unrealistic neglecting of the transverse shear stress component, minimize shear stress influence which "softenes" the finite element solution, so it may instantly undergo apparently higher deflections. This explains fast convergence of the different plate elements known in the literature, also. From the present example, we may draw the conclusion that by zeroing the stress components on clamped edge following the

assumptions of the plane theory, we may simulate the plane theory itself. From the reason that it is known that these stress components are not in fact equal to zero, but "much lesser" than other stress components, we prove that they can not be neglected, because it smears the real stress picture, in which stress concentration point is inside the plate in the vicinity of clamped edge.

5.1.2 Clamped circular plate

In the present example we will also show that by the use of the full mechanical theory that, the usual premise that stress concentration point of a clamped plate is on the clamped edge is not correct.

A clamped circular plate model problem [16] with edge length $a=1$ and thickness $t=0.01$, subjected to the uniform pressure $q=-1$, is considered. The Young's modulus is $E=9.81\cdot10^{10}$, and Poisson's ratio is $\nu=0.3$.

The visualization of the stress pattern for the F the case A, that is, full theory, is shown in Figures 6 and 7. We can see that stress concentration point is not at the clamped edge, but in its vicinity:

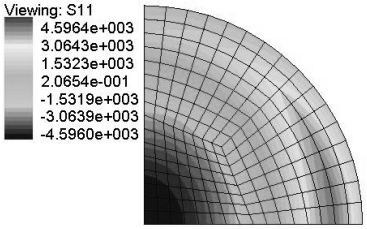

Fig.6. Case A: the stress concentration point

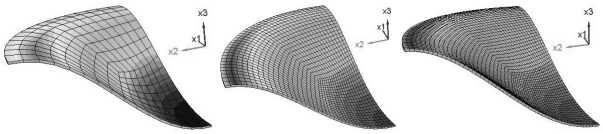

Fig. 7. Case A: Deflection and t^{xy}, FE meshes.

The visualization of the stress pattern, where plane theory assumptions that shear stress components are neglected, case B, is shown in Figure 8. We can see that stress concentration point is at clamped edge.

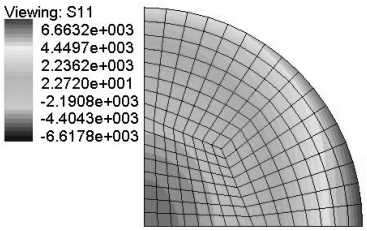

Fig. 8. Case B: the stress concentration point

5.1.3 Clamped plates - conclusions

With the visual inspection of the results in the present and former example, we can see that stress concentration point is always at the interface between the second and third row of the FE mesh. That is, that place of the stress concentration point converges to the clamped edge. Therefore, conclusion is that clamped engineering components must be strengthened in the vicinity of clamped edge, instead to have a hole for rivets as in airplane industry. The example is aircraft accident of the Aloha Airlines Flight 243 - Maui Hawaii, April 28, 1988 [17], when a major portion of the upper crown skin and structure of section 43 separated in flight causing an explosive decompression of the cabin. The damaged area extended from slightly aft of the main cabin entrance door. The cause is fatigue failure along lap joint S-10L. The root cause of the problem was failure of an epoxy adhesive to bond the aluminium sheets of the fuselage together when the B737 was manufactured. Where it failed to bond the two surfaces together, water could enter the gap and start the corrosion process. Since the corrosion products have a larger volume than the underlying metal, the two sheets were forced apart, putting extra stress on the rivets also used to hold them together. The present explanation is that rivets were plased also on the stress concentration points which inflated all of the above mentioned problems.

5.2 Simply supported circular plate

A simply supported circular plate [18] under uniform normal pressure $p=1$ shown in Figure 9, is analyzed. The radius of the plate is $r=5$ and thickness of the plate is $t=0.1$. The material is isotropic, modulus of elasticity is E=1092000 and Poisson's ratio is $\nu=0.3$. The plate theory solution for the central displacement and maximal radial stress component in the centre of the plate are w = -0.398137 and $t^{rr}=3093.75$ [16], respectively. The model problem has two planes of symmetry. Therefore, one-quarter is analysed, only. The resulting finite element mesh is distorted. The present model problem is discretized by the two layers of brick finite elements HC8/9 per thickness, that is $N\times N\times 2$. The essential boundary conditions per displacements and stresses, for case A, are given in the Figure 9.

We will also examine case B, where degrees of freedom of transversal shear stress components are suppressed (zeroed), as in the case of *plate theories*.

For comparison, the convergences of results are shown in Figure 10. Results are compared with the low order plate bending finite element with thickness change and enhanced strains, proposed by Piltner and Joseph in [18].

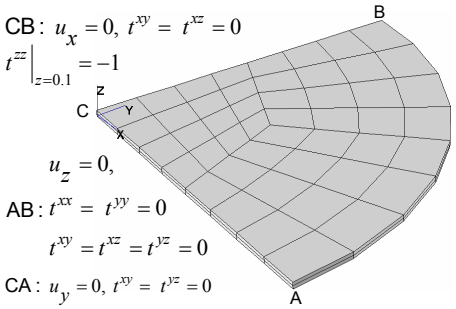

Fig. 9. Circular plate: boundary conditions

From Figure 10 we may see that both analyzed cases (Case A and Case B), converge to the same value, which is a little bit lower than one obtained by the Kirchhoff's plate theory. The fast convergence of the Case B is explained by the same analysis as the case of previous example. This explains fast convergence of the considered *Piltner's* plate element, also. On the issue of stress recovery of primal FE approaches, reader can learn more from [19].

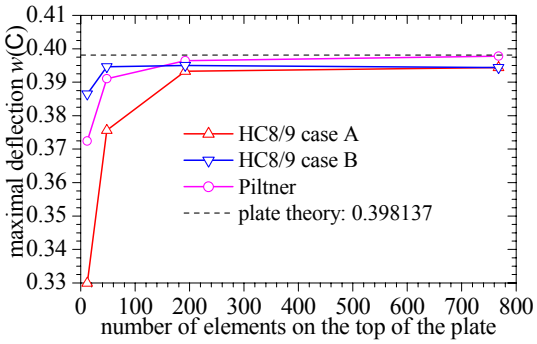

Fig. 10. Circular plate: maximal deflection

Next, the stress convergence is analyzed according to the target stress result from [18]. We may see that both present cases, Case A and Case B, converge to the same value that is about 10% higher than target result, which is shown in Figure 11. It is in accordance with [20] where it is said "*Comparison of the test and analytical results reveals that the stiffnesses of the dowel-fastened panels are between 10 and 20 percent greater than the analytically determined stiffnesses of the simply supported models*."

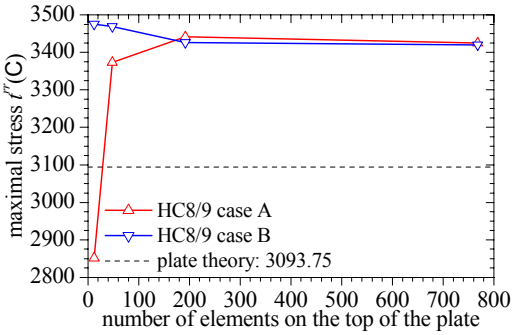

Fig. 11. Circular plate: maximal stress

5.3 Thermal barrier coating

A hollow long steel shaft coated by a bond layer and a ceramic layer shown in Fig. 12, is analyzed. Thermal conductivity of the steel and bond is $k = 25W/(mK)$. Thermal conductivity of the ceramics is $k = 1W/(mK)$. The outer and inner radii of shaft are $r_0 = 0.1m$ and $r_3 = 0.005m$. It is assumed that height is $h = 0.1m$. Five model problems with decreasing thickness t of coating (bond and ceramic), varied from $10^{-2}m$ to $10^{-6}m$, are presently considered. Thus, for the last example we are entering the area of the multiscale analysis. The temperature boundary conditions are prescribed: on the inner and outer surfaces, $T_3 = 500^0C$, and $T_0 = 1000^0C$, respectively.

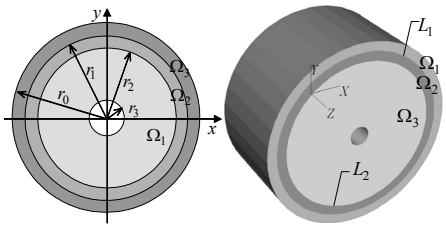

Fig. 12. Thermal barrier coating model problem

The results obtained by present finite element configurations HC8/9 and HC20/21 are compared with results obtained by two-dimensional conventional boundary element approach (CBEM) and analytical (target) results, which are reported in [21]. One-eight segment of the cylinder is analyzed due to the symmetry of geometry and thermal loading. All five model problems are discretized by only eight finite elements along circumference, and one finite element layer along height. The results of the thermal stress analysis are shown in Fig. 13. From the present example, we may see that present approach retain accuracy toward micro sized finite elements.

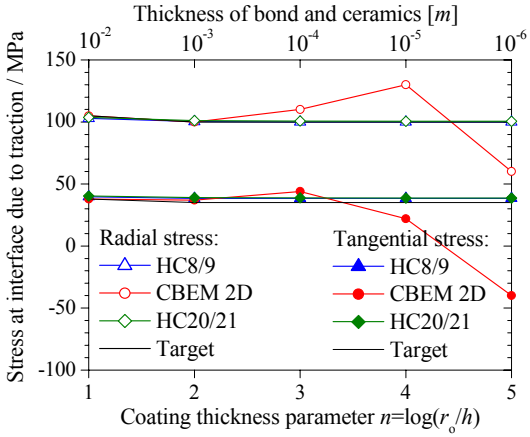

Fig. 13. Coating model: Mechanical induced stress

6 Nano-indentation

Despite the fact that the continuum mechanics (including finite element method) have yielded many useful results and continue to be the workhorse of applied mechanics - notably in industry, the continuum viewpoint of the fracture is inherently limited to the extent that it neglects the atomistic structure of solids [22].

A model problem of the quasi-static nano-indentation [20] shown in Figures 15 and 15, is considered. Namely, in MD simulation an atomically sharp rigid indenter is coming into contact with an ideally flat substrate. The substrate material is considered to be Titanium with Young's modulus $E = 116GPa$ and Poisson's ratio $\nu = 0.36$. The dimensions of the whole model problem (the CM domain and the MD patch embedded in it) are $2.02 \cdot 10^{-4} m \times 1.01 \cdot 10^{-4} m$. A domain of the model problem directly under the nanoindenter is calculated by the MD. The MD patch is of dimensions $1.16 \cdot 10^{-9} m \times 1.507 \cdot 10^{-8} m$.

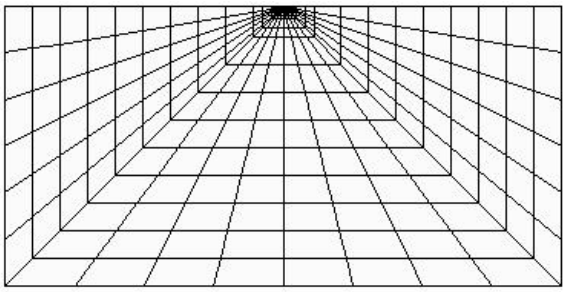

Fig. 14. Nanoidentation model problem

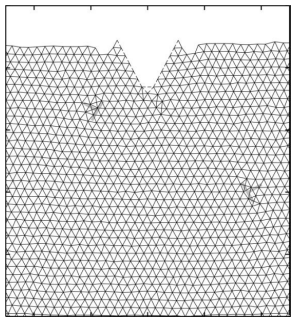

Fig. 15. Atomic configuration upon indentation

The MD analysis is performed on constant temperature of $100^0 C$ by using the Nose-Hoover thermosetting method (as presented in [23]). The MD part of the substrate is approximated by two-dimensional triangular lattice, which is equivalent to three-dimensional continuum under the plane strain conditions [13]. On the other hand, on the CM domain simulation is three-dimensional.

The transition from two-dimensional MD phase of simulation to the three-dimensional CM phase of simulation is performed by mirroring input values of MD displacements along the third dimension (i.e., along the thickness). Following equilibration, the intrusion of nano-indenter into the substrate takes place on the upper boundary of MD domain. It is important to emphasize that that this is an ongoing project, which renders a couple of simplifications necessary for the sake of the expedient code development. Specifically, the left and right boundaries of MD domain are free to deform, while the bottom boundary of MD domain is currently fixed. Also, the MD domain is admittedly miniscule at present—41×61 atoms—although order-of-magnitude larger MD ensembles are feasible on the PC used. At the onset of indentation, a dominant atomistic mechanism of plastic deformation is the local diffusional flow of the substrate atoms, resulting in their pile-up around the indenter tip ("wetting" of the tip). Subsequently, as the deformation energy accumulates around the tip, the edge dislocations are emitted from the tip region, as indicated in Fig. 15. The dislocations glide on their slip planes until they encounter the lateral (left and right) MD-region boundary, which results in formation of slip bands (slip discontinuities, dislocation steps). The formation of these bands is also captured by the localization of the deformation and stress fields of the CM region depicted in Figures 16 and 17.

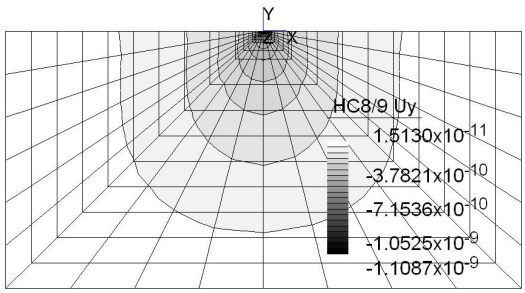

Fig. 16. u_y after first increment of analysis

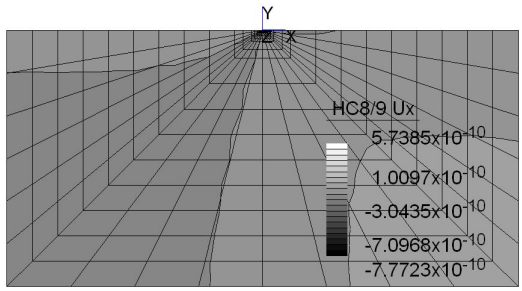

Fig. 17. u_y after first increment of analysis

It should be noted that in the present model problem the HC8/9 finite elements with maximal axial size ranging from size $3 \cdot 10^{-5}$ to size of $4 \cdot 10^{-8}$ are used without locking effects [8].

From Figures 16 and 17, we can see that there are no spurious behaviors of the results. Therefore, we can say that reliability of the present primal-mixed finite element approach harmonize bridging continuum and atomistic analyses in the multiscale materials modelling. More investigation on this subject is to be performed in future.

6.1 Hollow sphere with two materials and convective BC's

Sensitivity of the present approach to the presence of the material discontinuity is investigated in the present example. A model problem is the steady state heat transfer through a hollow bimaterial sphere [26]. Inner, interfacial and outer radius of the hollow sphere are $0.3m$, $0.35m$, and $0.37m$, respectively. The convection boundary conditions are prescribed on its inner and outer surface, such that $h_c^{\text{inner}} = 200\ W/m^2\,^\circ C$ and $T_a^{\text{inner}} = 70^0 C$, and $h_c^{\text{outer}} = 150\ W/m^2\,^\circ C$ and $T_a^{\text{outer}} = -9^0 C$, respectively. Thermal conductivities of the inner and outer material are $k^{\text{inner}} = 40 W/m^2\,^0 C$ and $k^{\text{outer}} = 20\ W/m^\circ C$. The target values are temperatures on three characteristic radii: inner, interfacial and outer, which are $T_{\text{A}} = 25.06^0 C$, $T_{\text{B}} = 17.84^0 C$ and $T_{\text{C}} = 13.16^0 C$, respectively.

Only one-eighth of the hollow sphere is presently analyzed due to the symmetry. The finite element configurations used were HC8/9, HC8/15, HC8/27, HC20/21 and HC20/27, and raw primal one H8. The sequence of models with uniform meshes refinement in all directions, were investigated. The coarsest mesh is shown in Fig. 8. Relative errors of calculated temperatures on characteristic radii at point B versus the number of finite elements in the mesh, is shown in Fig. 18. The obtained results reveal that all considered finite element configurations have high accuracy. In addition, artificially enforced continuity of heat flux shape functions along discontinuity surface of the abrupt material change (Point B) does not deteriorate results. Nevertheless, quadratic finite element configurations H20, H20/21 and H20/27 have relative error less than 0.01% immediately after the second discretization, which points out to the high accuracy of these configurations. It can be seen that very good results are obtained even with small number of elements in radial direction.

Further, the time efficiencies, i.e. execution time versus number of degrees of freedom, of HC8/9 finite element configuration (see Fig. 8) in connection with several presently considered solution schemes, are shown in Fig. 10.

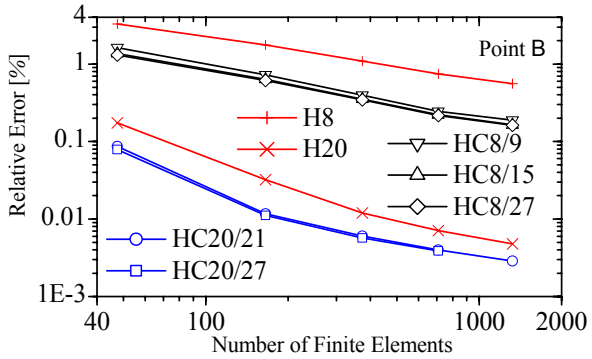

Fig. 18. Hollow sphere - uniform refinement: relative errors

From results reported in Fig. 19, it can be seen that MA47+MC30 procedure [6] is far more time efficient than other presently considered solution procedures, i.e. it is fifty times faster than simple Gaussian elimination procedure and twenty-five times faster than MA47 procedure, on the same computer platform.

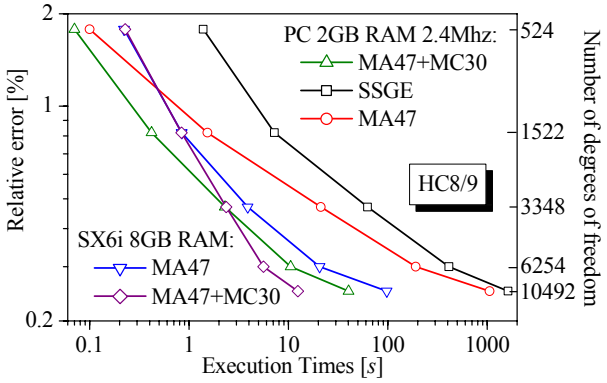

Fig. 19. Hollow sphere: time efficiency

7 Conclusion

From the results of the above analysis we may see that dimensional reduction as the source of inevitable errors has to be abandoned in the future. Instead it, fully reliable three-dimensional numerical simulation should be utilized. Forward that opinion, it is proven that reliable primal-mixed multifield finite element approach HC8/27 in semi-coupled thermo-mechanical analysis, follows the physical behavior of the real structures more closely than plane theories at the same time being time efficient. It was shown that it give us new insight in the behavior of the thin bodies, not possible by the plane theories. Further, it was shown that it trace stress pattern more accurately than plane theories. More, it is shown that present approach retains accuracy deep toward micro scale. It is shown that HC8/9 finite elements are used in multiscale analysis model problem, with finite element maximal axial size ranging from $3 \cdot 10^{-5}$ to $4 \cdot 10^{-8}$ meters, without locking effects [8].

References:

[1] Zienkiewicz OC, Taylor RL *The Finite Element Method* VOL I, McGraw–Hill, London, 1989

[2] Robey TH The Primal Mixed Finite Element Method and the LBB Condition, *Numerical Methods for Partial Differential Equations.* 8, 1992, pp. 357-379

[3] Arnold DN. Mixed finite element methods for elliptic problems, *Computer Methods in Applied Mechanics and Engineering*, 82, 1990, pp.281-300

[4] Babuska, I. On a dimensional reduction method. III, A-posteriori error estimation and an adaptive approach, *Math. Comp.,* 37, 156, 1981, pp. 361-383 (with M. Vogelius),

[5] Icardi U. Layerwise mixed element with sublaminates approximation and 3D zig-zag field, for analysis of local effects in laminated and sandwich composites. *International Journal for Numerical Methods in Engineering*. on line first, 2006

[6] Schmauder S Computational Mechanics Annu. Rev. Mater. Res. Vol.32, 2002, pp.437–65

[7] J. Djoko, B. Lamichhane, D. Reddy, B. Wohlmuth. Conditions for Equivalence between the Hu-Washizu and Related Formulations, and Computational Behavior in the Incompressible Limit, *Computer Methods in Applied Mechanics and Engineering*, Vol.195, 2006, pp. 4161-4178

[8] V. A. Maksimyuk1 and I. S. Chernyshenko1, Mixed functionals in the theory of nonlinearly elastic shells. Volume 40, Number 11 / November, 2004, *International Applied Mechanics*, Springer New York

[9] Duff IS, Erisman AM, Reid JK. *Direct methods for sparse matrices.* Oxford University Press, London, 1986

[10] Ghoniem NM, Busso EP, Kioussis N, Huang H. Multiscale modelling of nanomechanics and micromechanics: an overview. *Philosophical Magazine*, 1 Nov–1 Dec 2003, Vol. 83, Nos. 31–34, pp. 3475–3528

[11] Mijuca D. On hexahedral finite element HC8/27 in elasticity. *Computational Mechanics* 33(6), 2004, pp.466-480

[12] Mijuca D, Mastilović S. A Novel One-To-One Multiscale Approach to Computational Mechanics of Materials, *1st International Workshop on Nanoscience & Nanotechnology IWON2005,* 2005, pp. 180-186,

[13] Mijuca D, Ziberna A and Medjo B, A Novel Primal-Mixed Finite Element Approach for Heat Transfer in Solids, Computational Mechanics, *Computational Mechanics*, on-line first, 2006

[14] Shepherd MS, Finite element modelling within an integrated geometric modelling environment: Part II Attribute specification, domain differences and indirect element types. *Engineering with Computers* 1, 1985., pp.73-85,

[15] Duff IS, Reid JK. The multifrontal solution of indefinite sparse symmetric linear systems, *ACM Transactions on Mathematical Software* 9, 1983, pp.302–325

[16] Timoshenko S, Goodier JN, Theory of elasticity, McGraw–Hill, New York, 1970

[17] http://en.wikipedia.org/wiki/Aloha_Flight_243 #Aftermath

[18] Piltner R, Joseph DS. An accurate low order plate bending element with thickness change and enhanced strains. *Computational Mechanics* 27: 2001, pp. 353-359

[19] Mijuca D, Berković M. Stress recovery procedure based on the known displacement, *Facta Universitatis, Series Mechanics, Automatic control and Robotics*, Vol.7, No.2, 1997, pp. 513-523

[20] W. H. Thomas. Modelling the influence of boundary conditions on the concentrated load performance of oriented strand board floor decking. *Holz Roh Werkst,* 2004 62:44–49

[21] Lu S, Dong M. An advanced bem for thermal and stress analyses of components with thermal barrier coating, *Electronic Journal of Boundary Elements*, 1, 2003, pp. 302-315

[22] Ghoniemy NM,Esteban P. Busso EP, Kioussis N,Huang H. Multiscale modelling of nanomechanics and micromechanics: an overview, *Philosophical Magazine.,* 83: 2003, pp. 3475-3528.

[23] Holian BL, Voter AF, and Ravelo R. Thermostatted molecular dynamics: How to avoid the Toda daemon hidden in Nose-Hoover dynamics, *Physical Review* E 52 (3): 1995, pp.2338-2347.